Ecole Centrale de Nantes

MASTER CORO-IMARO

Human Motion for Humanoid Control

Lab Report

Serena Roncagliolo, Camille Vindolet

25 November 2020

Contents

1 Introduction

The main objective of this laboratory is to collect and analyse body measurements data taken from a subject in order to simulate motion on a simulated humanoid subject.
Due to the present health crisis, the measurements of the body segments were not performed, but were provided with the subject. By using given data of the 41 body segments parameters (BSP) we managed to build the *modified Hanavan Model*, the geometric human body model designed by Hanavan (1964).
We were given the measurements of 5 different groups, with the result of the mean value and the standard deviation of collected data.
We were then given a set of files containing data collected while the subject performed different movements such as waving one hand. Those files contained the position and angle of each body segment and could thus be used to simulate the mannequin displacement. Moreover another set of files contained the measured ground reaction forces and moments in the performing of each of those same movements. We computed the theoretical ground reaction forces and moments and compared them to the ones obtained by measurement.

2 Human body model

A body segment dimension should depend on several factors such as gender, age, population and body configuration. However in a Human body model, the body segments dimensions are extracted from measurements of some Body Segment Parameters (BSP). The estimation of BSP measurements lead to:

- dimensions
- mass (including density)
- Centre of Mass (CoM) position
- Inertia matrix

There are different models and methods to use and measure the BSP. They are not adapted to the shape of the human body since there is no difference taken into account between men and women, a young and an old subject, people from different origin, people of different musculature, in terms of mass distribution and density. Each model gives different outputs but none give exact ones.
In our case we applied the modified Hanavan model and we will present the creation of the body segments and their characteristics from this.

2.1 Modified Hanavan Model (1964)

This model is inspired from the work of Hanavan carried out in 1964 in the article *A mathematical model of the human body*. In this model, the segment masses are estimated using the regression equations described by Clauser et al. in 1969 instead of the equations of Barter presented in 1957. This new approach was originally tried by Miller and Morrison in 1975. As for the Hanavan Model, the body is segmented and each segment is given a shape to describe it. The Hanavan Model segmentation is described in figure 1. The differences with the Hanavan Model regarding the body segments include:

- the trunk is considered as 3 segments separated at the omphalion (navel) and xyphion level to take into account differences in mass distribution of these segments, giving:
  - upper trunk: elliptical column
  - middle trunk: elliptical solid
  - lower trunk: elliptical column
- the hand is defined as an ellipsoid of revolution
- the foot is defined as an elliptical solid with the base being circular
- the thigh is defined as an elliptical solid with the top being circular

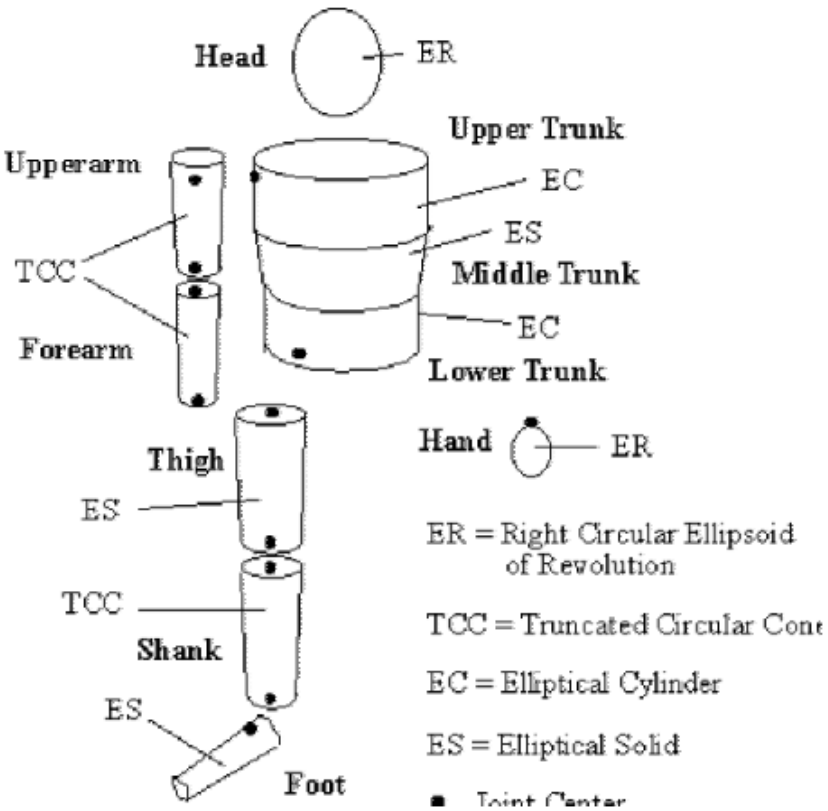

Figure 1: Modified Hanavan Model

In order to compute the dimensions of each one of the building blocks of the model, several parameters are defined: P_1 to P_{41}. They are called "body segment parameters" (BSP) and their definition is shown in Fig. (2). The measurement and estimation of these BSP is explained later on.

1	Length, Hand	**21**	Circumference, Toe
2	Length, Wrist to Knuckle	**22**	Circumference, Ankle
3	Length, Forearm	**23**	Circumference, Shank
4	Length, Upperarm	**24**	Circumference, Knee
5	Length, Elbow to Acromion	**25**	Circumference, Upper Thigh
6	Length, Foot	**26**	Circumference, Head
7	Length, Shank	**27**	Circumference, Chest
8	Length, Thigh	**28**	Circumference, Xyphion Level
9	Length, Head	**29**	Circumference, Omphalion Level
10	Length, Upper Trunk	**30**	Circumference, Buttock
11	Length, Xyphion to Acromion Level	**31**	Width, Hand
12	Length, Middle Trunk	**32**	Width, Wrist
13	Length, Lower Trunk	**33**	Width, Foot
14	Fist	**34**	Width, Toe
15	Wrist	**35**	Width, Toe
16	Forearm	**36**	Width, Chest
17	Elbow	**37**	Width, Xyphion Level
18	Axiliary Arm	**38**	Width, Ombphalion Level
19	Foot	**39**	Coxae
20	Foot	**40**	Lenght, XyphionLevel to Chin/Neck Intersection
41	Hip to Chin/Neck intersection = $_P12 + P_13 + P_40$		

Figure 2: Anthropometric Parameters Used in the Modified Hanavan Model

2.2 Body segments characteristics

The model of the Human Body (geometry and mass distribution) is obtained by applying the equations in Fig. (3) and Fig. (4). In Fig. (3) we define the geometric parameters of the shapes of each segment in function of the BSP and in Fig. (4) we define the mass of each segment in function of the BSP. For the geometric parameters the BSP distances are converted in millimetres. In the mass computation we multiply each BSP by 100 as those distances were given to us in meters and we use them here in centimetres. In the following equations we define:

- **EC** = Elliptical Column
- **ER** = Ellipsoid of Revolution
- **ES** = Elliptical Solid
- **SE** = Semi-Ellipsoid
- **TCC** = Truncated Circular Cone
- $a, a_0, a_1, b, b_0, b_1, c$ and L = the shape parameters as defined in figures 5 and 6

An example of the hand model can be explicitly given as it is used in the hanavan.m file:

$$R_{Hand} = body \tag{1}$$
$$R_{Hand}.name = "R_{Hand}" \tag{2}$$
$$R_{Hand}.a = 1000\frac{P(14)}{2pi} \tag{3}$$
$$R_{Hand}.b = R_{Hand}.a \tag{4}$$
$$R_{Hand}.c = 1000\frac{P(2)}{2} \tag{5}$$
$$R_{Hand}.mass = 0.038 * P(15) * 100 + 0.08 * P(32) * 100 - 0.66 \tag{6}$$

Segment	Geometric Shape	Group	Arguments of the BSP Functions
Hand	ER	SE	$a = b = \frac{P_{14}}{2\pi} \quad c = \frac{P_7}{2}$
Forearm	TCC	ES	$a_0 = b_0 = \frac{P_{17}}{2\pi} \quad a_1 = b_1 = \frac{P_{15}}{2\pi} \quad L = P_3$
Upperarm	TCC	ES	$a_0 = b_0 = \frac{P_{18}}{2\pi} \quad a_1 = b_1 = \frac{P_{17}}{2\pi} \quad L = P_5$
Foot	ES with Circular Base	ES	$a_0 = b_0 = \frac{P_{19}}{2\pi} \quad a_1 = \frac{P_{33} + P_{34}}{4} \quad b_1 = \frac{P_{20} + P_{21}}{2\pi} - a_1$ $L = P_8$
Shank	TCC	ES	$a_0 = b_0 = \frac{P_{24}}{2\pi} \quad a_1 = b_1 = \frac{P_{22}}{2\pi} \quad L = P_7$
Thigh	ES with Circular Top	ES	$b_0 = \frac{P_{35}}{2} \quad a_0 = \frac{P_{25}}{\pi} - b_0 \quad a_1 = b_1 = \frac{P_{24}}{2\pi}$ $L = P_9$
Head	ER	SE	$a = b = \frac{P_{26}}{2\pi} \quad c = \frac{P_9}{2}$
U Trunk	EC	ES	$a_0 = a_1 = \frac{P_{36} + P_{37}}{4} \quad b_0 = b_1 = \frac{P_{27} + P_{28}}{2\pi} - a_0 \quad L = P_{11}$
M Trunk	ES	ES	$a_0 = \frac{P_{37}}{2} \quad a_1 = \frac{P_{38}}{2} \quad L = P_{12}$ $b_0 = \frac{P_{28}}{\pi} - a_0 \quad b_1 = \frac{P_{29}}{\pi} - a_1$
L Trunk	EC	ES	$a_0 = a_1 = \frac{P_{38} + P_{39}}{4} \quad L = P_{13}$ $b_0 = b_1 = \frac{P_{29} + P_{30}}{2\pi} - a_0$

Figure 3: Geometric Shapes and Arguments of the BSP estimation

Mass prediction equations

Segment	Prediction Equation
Hand	$m = 0.038*P_{15} + 0.080*P_{32} - 0.660$
Forearm	$m = 0.081*M + 0.052*P_{16} - 1.650$
Upper arm	$m = 0.007*M + 0.092*P_{18} + 0.050*P_5 - 3.101$
Foot	$m = 0.003*M + 0.048*P_{22} + 0.027*P_6 - 0.869$
Shank	$m = 0.135*P_{23} - 1.318$
Thigh	$m = 0.074*M + 0.138*P_{25} - 4.641$
Head	$m = 0.104*P_{26} + 0.015*M - 2.189$
Whole trunk	$m_{wt} = 0.349*M + 0.423*P_{41} + 0.229*P_{27} - 35.460$
Upper trunk	$m = 0.92*V_{ut}*sf$
Middle trunk	$m = 1.01*V_{mt}*sf$
Lower trunk	$m = 1.01*V_{lt}*sf$

M: Whole body mass; P_i: Anthropometric parameter i; V: volume.

Figure 4: Mass prediction equations with $s_f = \frac{m_{wt}}{0.92*V_{ut}+1.01*(V_{mt}+V_{lt})}$ the scaling factor

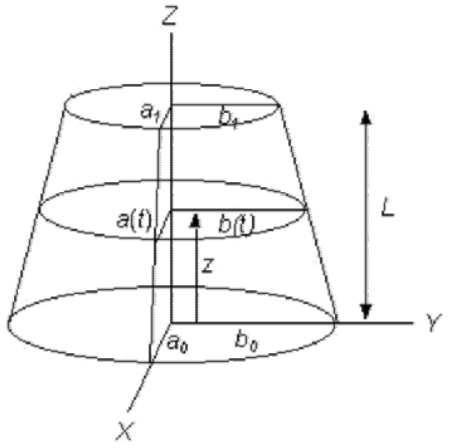

Figure 5: Elliptical Solid shape definition

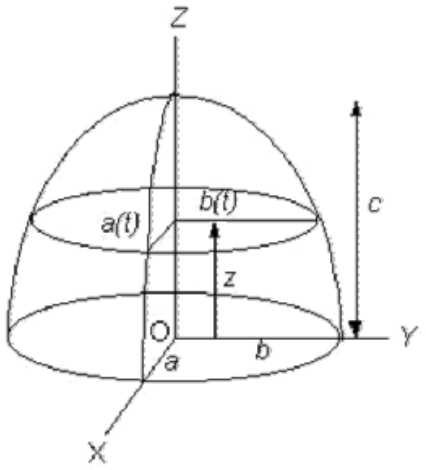

Figure 6: Semi-Ellipsoid shape definition

2.3 Human Body dynamic parameters

It is possible to compute the volume, the mass distribution and the inertia of each body segments previously defined. All these body segments are given a type to either build an Ellipsoid or an Elliptical shape from the previous geometric parameters and the mass computed in the *Body segments characteristics* sub section. Those computations are different for Ellipsoid and for Elliptical. They are given in figures 8 and 7 and they will be used for the Newton Euler calculation. For the Elliptical solid the properties we first need to define are:

$$A_1^{ab} = \frac{B_1^{ab}}{3} + \frac{B_2^{ab}}{2} + B_3^{ab}$$

$$A_2^{ab} = \frac{B_1^{ab}}{4} + \frac{B_2^{ab}}{3} + \frac{B_3^{ab}}{2}$$

$$A_3^{ab} = \frac{B_1^{ab}}{5} + \frac{B_2^{ab}}{4} + \frac{B_3^{ab}}{3}$$
$$A_4^{abcd} = \frac{B_4^{abcd}}{5} + \frac{B_5^{abcd}}{4} + \frac{B_6^{abcd}}{3} + \frac{B_7^{abcd}}{2} + B_8^{abcd}.$$

and

$$\begin{aligned} B_1^{ab} &= (a_1 - a_0) \\ B_2^{ab} &= a_0(b_1 - b_0) + b_0(a_1 - a_0) \\ B_3^{ab} &= a_0 b_0 \\ B_4^{abcd} &= (a_1 - a_0)(b_1 - b_0)(c_1 - c_0)(d_1 - d_0) \\ B_8^{abcd} &= a_0 b_0 c_0 d_0 \end{aligned}$$

$$\begin{aligned} B_5^{abcd} = a_0(b_1 - b_0)(c_1 - c_0)(d_1 - d_0) + b_0(a_1 - a_0)(c_1 - c_0)(d_1 - d_0) \\ +c_0(a_1 - a_0)(b_1 - b_0)(d_1 - d_0) + d_0(a_1 - a_0)(c_1 - c_0)(b_1 - b_0) \end{aligned}$$

$$\begin{aligned} B_6^{abcd} = a_0 b_0(c_1 - c_0)(d_1 - d_0) + a_0 c_0(b_1 - b_0)(d_1 - d_0) + a_0 d_0(c_1 - c_0)(b_1 - b_0) \\ +b_0 c_0(a_1 - a_0)(d_1 - d_0) + b_0 d_0(c_1 - c_0)(a_1 - a_0) + c_0 d_0(a_1 - a_0)(b_1 - b_0) \end{aligned}$$

$$B_7^{abcd} = b_0 c_0 d_0(a_1 - a_0) + a_0 c_0 d_0(b_1 - b_0) + b_0 a_0 d_0(c_1 - c_0) + b_0 c_0 a_0(d_1 - d_0)$$

The volume of the body segment is extracted from $\rho = \frac{Mass}{Volume}$. For the Semi-Ellipsoid the volume is :

$$Volume_{SE\frac{1}{2}} = \frac{2\pi}{3} abc \tag{7}$$

For the Ellipsoid the volume is :

$$Volume_{SE} = \frac{4\pi}{3} abc \tag{8}$$

For the Elliptical Solid it is:

$$Volume_{ES} = L\pi A_1^{ab} \tag{9}$$

The position of the CoM is computed as expressed in figures 7 and 8 and from the marker position of the segment under consideration. The main axis of an Elliptical Segment is defined by the direction given by the current marker position and the following marker.

Mass	$\frac{2\pi}{3}\rho abc$
CoM pos	$\frac{3}{8}c$
I_{xx}	$\frac{1}{5}m[(b^2 + c^2) - (\frac{3}{8}c)^2]$
I_{yy}	$\frac{1}{5}m[(a^2 + c^2) - (\frac{3}{8}c)^2]$
I_{zz}	$\frac{1}{5}m(a^2 + b^2)$

Figure 7: Semi Ellipsoid shape mass distribution and inertia

Mass	$\pi\rho L A_1^{ab}$
CoM pos	$L\frac{A_2^{ab}}{A_1^{ab}}$
I_{xx}	$\frac{1}{4}m\frac{A_4^{abbb}}{A_1^{ab}} + mL^2\frac{A_3^{ab}}{A_1^{ab}} - m(L\frac{A_2^{ab}}{A_1^{ab}})^2$
I_{yy}	$\frac{1}{4}m\frac{A_4^{aaab}}{A_1^{ab}} + mL^2\frac{A_3^{ab}}{A_1^{ab}} - m(L\frac{A_2^{ab}}{A_1^{ab}})^2$
I_{zz}	$\frac{1}{4}m\frac{A_4^{aaab}+A_4^{abbb}}{A_1^{ab}}$

Figure 8: Elliptical Solid shape mass distribution and inertia

2.4 BSP estimation

Because of the COVID-19 crisis we used the results of the measured BSP from five groups of the previous year. Those results are exposed in figure 9. We also have the computed mean of these five groups BSP measures in the graph of figure 10. Later on we use the mean values of the BSP as the true values for this experiment. Indeed those measurements are not very accurate as they depend on a lot of external unpredictable factors: the actor can move a little, the eyes may not be perfectly aligned with the measure value, the measurement to take might not be well positioned, and the way to measure may be different from one group to an other as it was not described explicitly in the hanavan model..etc. This is the reason why all the groups have found different values. Moreover the standard deviation computation for each BSP measurement is in figure 11. When a standard deviation value is too important we check that there isn't a value too different from the rest of them. In the table we received one value was deleted for group 5 parameter 41. This may be because the value measured was too different from the others, and was thus deleted, or because the group didn't succeed to measure this parameter which corresponds to the length going from the hip to the chin. It can be computed using parameter 40, the length going from the Xyphion Level to the Chin, which was not measured either.

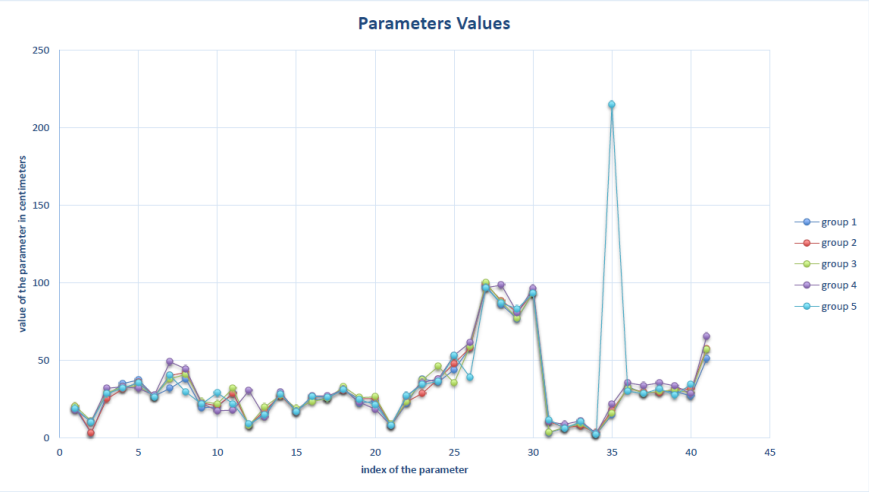

Figure 9: BSP values measured by 5 groups

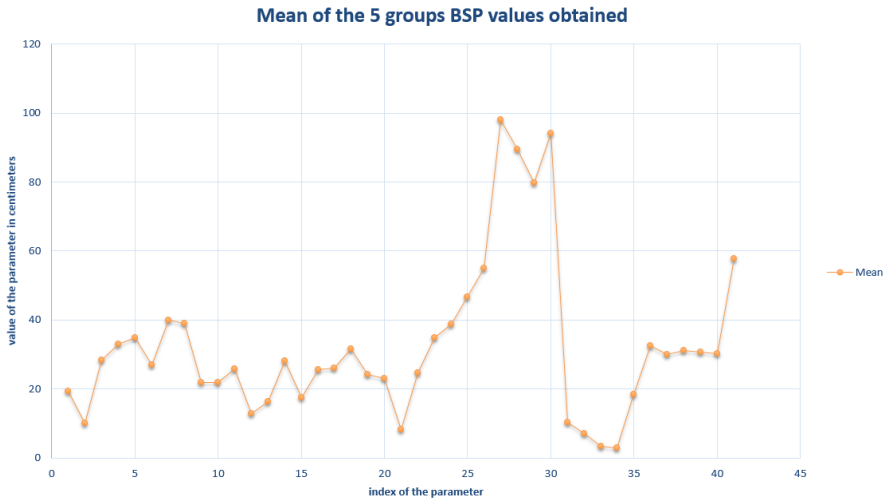

Figure 10: Mean of the BSP values measured by 5 groups

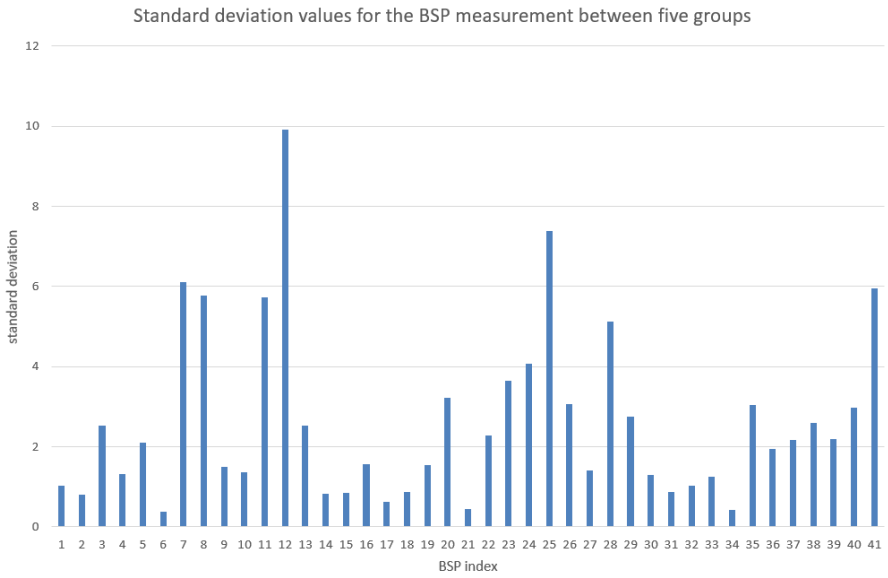

Figure 11: Standard deviation of the BSP values measured by 5 groups

We use the BSP mean measured to create the semi-Ellipsoid and Elliptical shapes of the body segments in the animation. In addition we use the BSP to compute the dynamics of the observed body. Indeed we will build efforts from the kinematics and BSP measurements.

3 Motions and forces measurements and computation to control a humanoid

In this section we are provided with data describing different motions which were carried out by an actor. We use the files to analyse them and check the validity of our model in order to understand if the measured human motions can be used to control a humanoid robot or

simulation.

3.1 Understanding and using provided data

During last year laboratory sessions an actor performed several motions. Those were monitored and measured to extract valuable data that could be applied later on to control a humanoid. These are the data we now want to understand and see in which way it can be used to apply such a control. The given motions are the following:

- particular motions defined by the groups who took the measurements (custom, custom2, customL)
- arm motions executed at different velocities (slowArm, mediumArm, fastArm)
- leg motions executed at different velocities (slowKick, mediumKick, fastKick)
- leg motions with arm motions (slowKickArm, mediumKickArm, fastKickArm)
- vertical jumps with and without counter movement (jumpFeetUp, medJump, quickJump, maxJump, maxJump2)

These motions are defined in order to facilitate the observation of the trajectories, velocities, accelerations and overall joint behaviour of each one of the human body segments.
The ground reaction forces and moments measurements are provided in .csv files recorded by the force plate Dtrack devices. The kinematics from motion capture is recorded in the 4 motions data folders containing 18 drf files with the same titles as the .csv files since they correspond to the same motions. They contain the positions (x,y,z) and Euler angles of each body segment along a reference frame. They are recorded by A.R.T. optical tracking system assisted by ART-Human application. We assume the devices used for motion capture were correctly calibrated.

How to read the drf data files Each .drf data file contains the following parameters:

- *frame counter (fr)*
- *timestamp*
- *identifiers 6d*: these data provide the coordinates of the bodies expressed in a relative frame (each body is related to the precedent body). It is difficult to use these data, we would have to understand the links and joints between the bodies and define a pivot point to their rotations
- *identifiers 6dj*: we take the data given after these identifiers. The data are expressed in the absolute frame, as [id num] where *num* gives the number of bodies. It is followed by:
  - a vector of 6 elements: that contains coordinates x,y,z and angular positions
  - a vector of 9 elements, which we don't use

In order to understand which vector of data correspond to which body, we have computed a custom function which plots the markers as shown in Fig. (12)

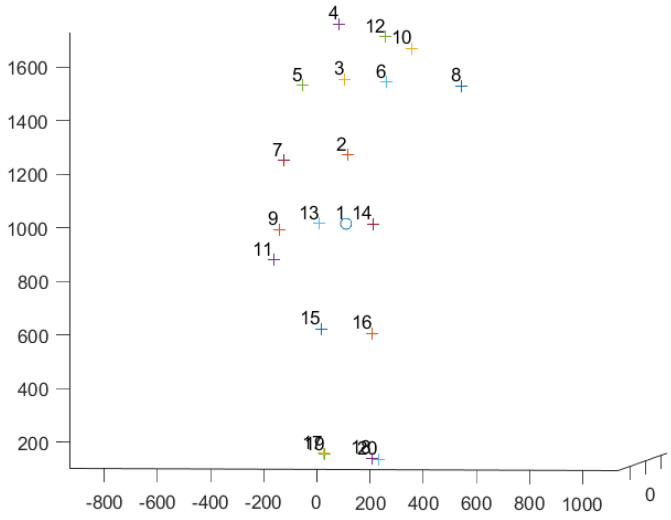

Figure 12: Plot of markers

The translations of the markers positions defined in the absolute frame are given by the x,y,z positions of the 6 elements vector after the *6dj* identifier and for each body segment. They are the first three coordinates of this vector. The 3 following angular values in this same vector corresponds to Euler angles in the order X, Y, Z. This was determined by applying rotations on the ellipsoid and elliptical segments surfaces with the function rotate from Matlab. We translated the drf files into data exploitable in the code. This is done in the read.m file. At the time this file was made it wasn't known which set of data were going to be used: the ones after the *6d* identifier or the ones after the *6dj* identifier. The file read.m creates a variable *motion* of size 3x20. In it, can be found the variables defined in the relative frames in a variable called q, the variables defined in the absolute frame in a variable called J, all of the time of data recordings in t, and all of these three type of elements for each of the 20 bodies. The variable J that we use is of size 6x835, and contains x,y,z,θ,α,γ, for the 835 times. The angle θ is about the X axis, the angle α is about the Y axis, the angle γ is about the Z axis. The variables x,y,z are the position coordinates in space in the absolute frame of the marker under consideration. The markers are:

- Marker 1: the lower trunk
- Marker 2: the middle trunk
- Marker 3: the upper trunk
- Marker 4: the head
- Marker 5: the left shoulder
- Marker 6: the right shoulder
- Marker 7: the upper left arm
- Marker 8: the upper right arm
- Marker 9: the left forearm
- Marker 10: the right forearm

- Marker 11: the left hand
- Marker 12: the right hand
- Marker 13: the left thigh
- Marker 14: the right thigh
- Marker 15: the left shank
- Marker 16: the right shank
- Marker 17: the left ankle
- Marker 18: the right ankle
- Marker 19: the left foot
- Marker 20: the right foot

3.2 Animation of a humanoid simulation using body segments markers displacement data recorded by motion capture

3.2.1 Creating the body segments for the animation

The humanoid we want to represent is made of 16 segments. The ankles and shoulders are not taken into consideration. The model is shown in figure (1).
The segments which compose our simulated humanoid, can be recreated by using ellipsoid or elliptical shapes.
Recreating ellipsoid shapes is quite simple, since Matlab already has a function implemented for this purpose, while, in order to recreate elliptical shapes, we had to create a custom class: we imagined an elliptical shape as made up of two ellipsis, the *base ellipse*, the *top ellipse* which are then connected together by a surface. The elliptical is constructed from the bottom base to the top one. Its "centre" value corresponds to the centre of the bottom ellipse.

3.2.2 Motion of the body segments

The translations of the centres of the ellipsoid and elliptical segments are defined as the translations of the markers. The rotations of the body segments are defined by applying an axis direction to the ellipsoids and ellipticals obtained by the line joining the segment marker to the next segment marker. Examples of the obtained animations are given in figures 13, 14, and 15. The motion in figure 13 is a waving motion of the right arm. The motion in figure 14 is a motion designed by last year students. The motion in figure 15 is a jump with two feet of the actor. This motion is interesting to analyse as it can be noticed that some data are lost in the recording of the motion. This is due to the fact that the markers are seen as light spots by the recording device. In jumping motions some markers conceal others, masking them for some time and the corresponding data are lost. Moreover the fast motions have the same problem since markers may not be successfully tracked by the device. The loss of data for the jumping motion can be seen in figure 16.

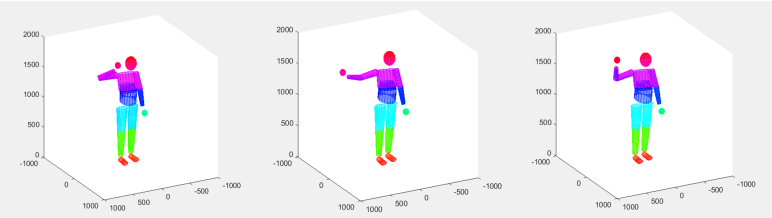

Figure 13: slowArm motion animation

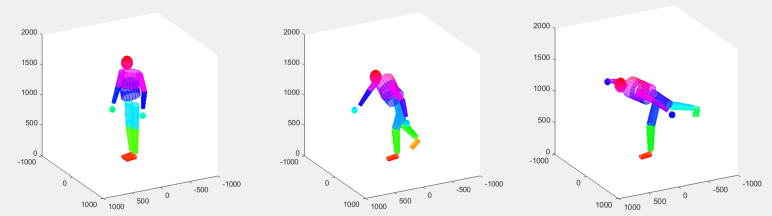

Figure 14: custom motion animation

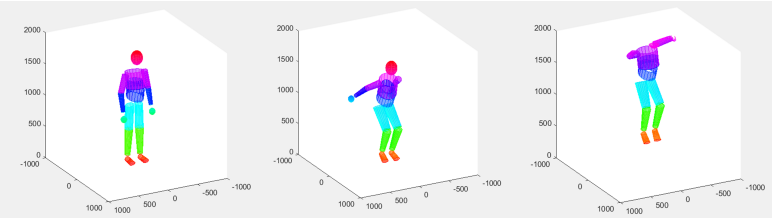

Figure 15: jumpFeetUp motion animation

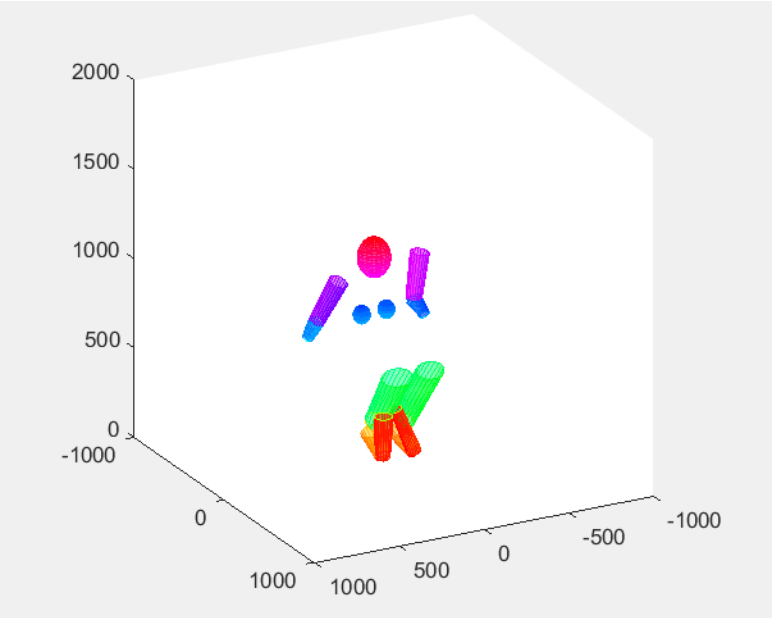

Figure 16: jumpFeetUp motion animation at a time of data loss

3.2.3 Algorithm for a motion of one body segment

Let's assume we want to create the displacement of an elliptical shape.
The first step is to create the shape. For this we create an instance of an object of the Elliptical Solid class, called ES, and we assign attributes to it: a0, a1, b0, b1, length, and a mass, as defined in figure 5. The mass is not used for the animation. Once the object is created we give it a shape by building it with the build.m function.
First the ellipses are shaped. Then they are oriented by taking into account the direction wanted for the solid under consideration. For this, and after many tries, we decided not to use the Euler Angles that were provided to us as we didn't know their exact definition and the methods we put into place to use them did not work. Instead we directed the solids by the vector connecting the solid marker to the next solid marker. For this we defined the rotation matrix built with the elevation and azimuth angles. The elevation angle is defined as follows:

$$E = arctan\left(\frac{z_2 - z_1}{\sqrt{(x_2 - x_1)^2 + (y_2 - y_1)^2}}\right) \tag{10}$$

The azimuth angle is:

$$A = arctan\left(\frac{y_2 - y_1}{x_2 - x_1}\right) \tag{11}$$

The rotation matrix is:

$$\begin{pmatrix} sin(E)cos(A) & -sin(A) & cos(E)cos(A) \\ sin(E)sin(A) & cos(A) & cos(E)sin(A) \\ -cos(E) & 0 & sin(E) \end{pmatrix} \tag{12}$$

We apply this rotation matrix to the ellipses. We create the unitary vector:

$$u = \frac{marker_2 - marker_1}{\|marker_2 - marker_1\|} \tag{13}$$

The first ellipse centre is positioned at the solid marker position (called marker 1 in the previous equation). The second ellipse is positioned at the solid marker position to which we add the length value of the segment under consideration. After this the solid ellipses are correctly oriented and positioned and the surface connecting the ellipses is made by the use of Matlab function "mesh".

3.3 Inverse Pendulum Model

3.4 Inverse Pendulum Model

3.4.1 Single Inverted Pendulum

Context We learnt in class that the motion of the Centre of Mass of the humanoid follow regular sinusoidal oscillations in the sagittal plane as shown in figure 17. Thus we can try to model this trajectory by a simple inverted pendulum model with a ground level fixed pivot point during midstance that we will suppose, is at the ankle.

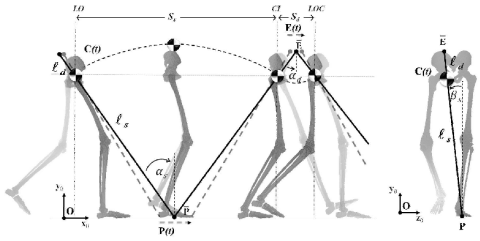

Figure 17: Trajectory of the CoM and Inverted Pendulum Model

The Single Inverted Pendulum schematic is presented in figure 18.

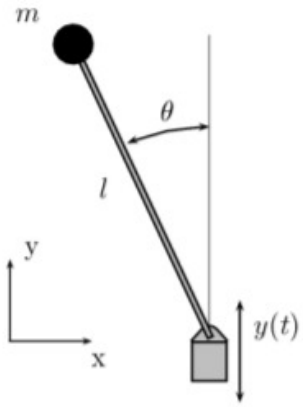

Figure 18: Single Inverted Pendulum schematic

We consider one torque control centered at the ankle joint, this control is grounded and the we suppose the mass of the whole pendulum centered at the CoM of the whole body (located at distance L from the ankle joint)

The total forces which are applied on the ground and the moment applied on the joint are given by:

$$F_x = 0 \tag{14}$$

$$F_y = mg \tag{15}$$

$$M_y = mgLsin\theta \tag{16}$$

The equations of the position of point m (of mass m) with respect to the origin depending on the angle position are given by

$$Position \begin{cases} x = lsin\theta \\ y = lcos\theta \end{cases} \tag{17}$$

The velocity of the mass point depending on the angle position and angular velocity is given by:

$$Velocities \begin{cases} \dot{x} = l \cdot cos(\theta) \cdot \dot{\theta} \\ \dot{y} = -l \cdot sin(\theta) \cdot \dot{\theta} \end{cases} \tag{18}$$

while the accelerations are given by:

$$Accelerations \begin{cases} \ddot{x} = l \cdot cos(\theta) \cdot \ddot{\theta} - l \cdot sin(\theta)(\dot{\theta})^2 \\ \ddot{y} = -l \cdot sin(\theta) \cdot \ddot{\theta} - l \cdot cos(\theta)(\dot{\theta})^2 \end{cases} \tag{19}$$

Forces and torques applied on it are given by:

$$Forces \quad and \quad moments \begin{cases} F_x = m\ddot{x} \\ F_y = m\ddot{y} + mg \\ M = l(F_x sin\theta + F_y cos\theta) \end{cases} \tag{20}$$

Observed results For the single pendulum, the first thing that can be observed on the *Pendulum Motion* graph is that the motion of the pendulum is a regular sinusoidal oscillations. This is a first clue that the code is correct since this is indeed the expected behaviour for a single inverted pendulum.
The ground reaction forces results could be used in two ways. First to check that our next Newton Euler ground reaction forces computation are correct in the case of the inverted pendulum so that we can validate our computations. Second to compare our theoretical results with the results obtained by measurements and validate or not the single inverted pendulum.

Possible amelioration It would have been interesting in the case of the pendulum to check the kinetic and potential energy of the pendulum as in this case there is, theoretically, no energy loss and the total energy is constant.

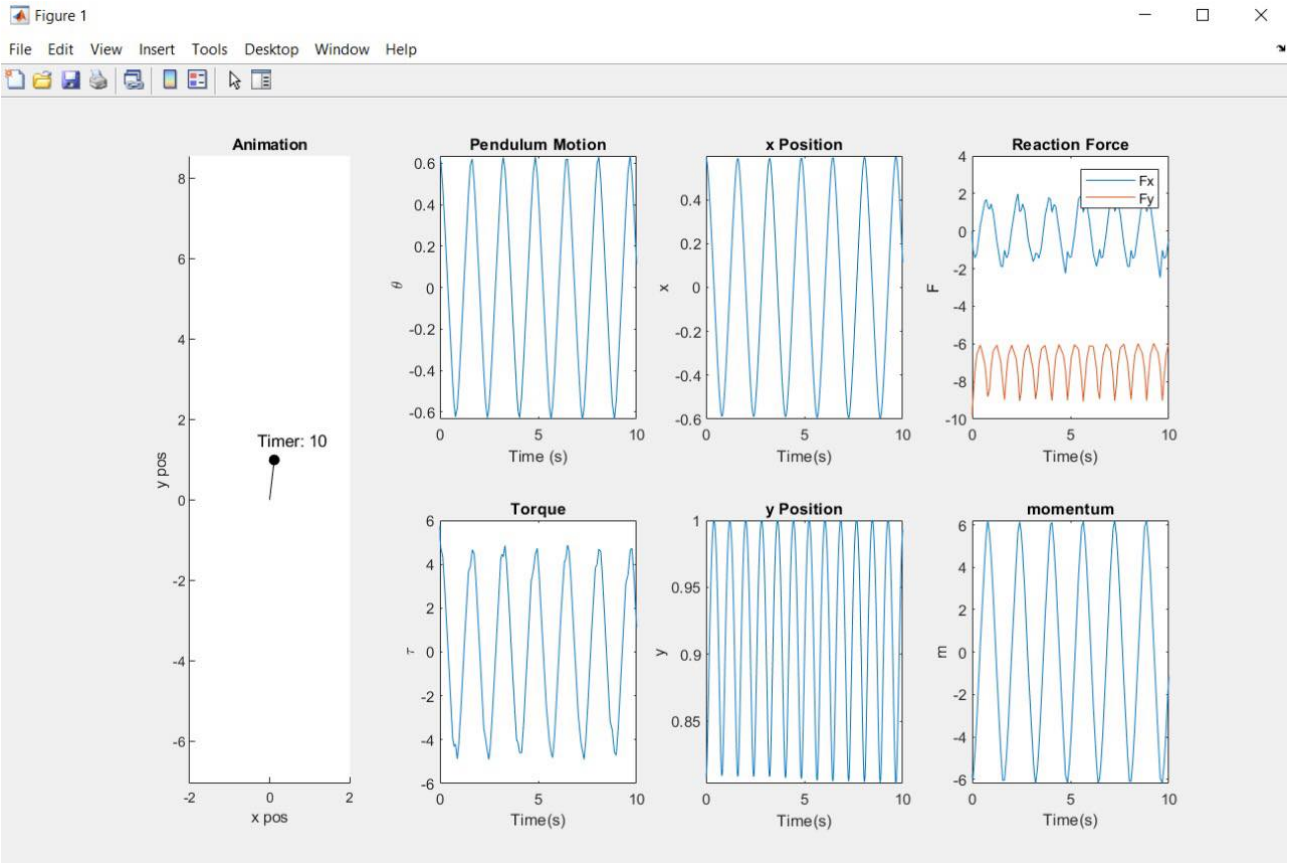

Figure 19: Single Inverted Pendulum results for forces, momentum and motion

3.4.2 Double Inverted Pendulum

It is possible to model the humanoid as a double inverted pendulum instead of the single inverted pendulum to take into account another center of rotation, the hip, relevant to the position of the CoM of human body walking. Balance in an Inverted Pendulum is more difficult and this is why this system can be interesting to study in the application to a humanoid robot, although single inverted pendulum may be enough to describe a humanoid motion of the CoM.
The double inverted pendulum schematic is presented in figure 20.

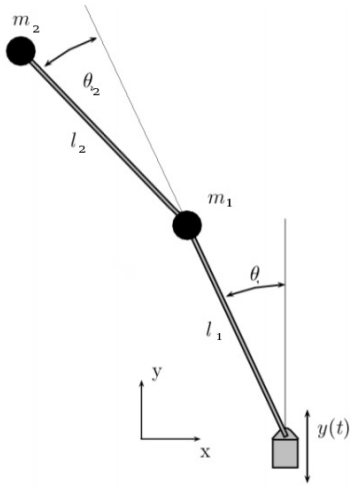

Figure 20: Double Inverted Pendulum schematic

The position, velocity, and acceleration for the two mass points are given respectively in equation 21, 22 and 23. The forces and moments applied on the mass points are given in equations 24 and 25.

$$Position \begin{cases} x_1 = l_1 sin\theta_1 \\ y_1 = l_1 cos\theta_1 \\ x_2 = l_1 sin\theta_1 + l_2 sin\theta_2 \\ y_2 = l_1 cos\theta_1 + l_2 cos\theta_2 \end{cases} \tag{21}$$

$$Velocity \begin{cases} \dot{x_1} = l_1 cos\theta_1 \dot{\theta_1} \\ \dot{y_1} = -l_1 sin\theta_1 \dot{\theta_1} \\ \dot{x_2} = l_1 cos\theta_1 \dot{\theta_1} + l_2 cos\theta_2 \dot{\theta_2} \\ \dot{y_2} = -l_1 sin\theta_1 \dot{\theta_1} - l_2 sin\theta_2 \dot{\theta_2} \end{cases} \tag{22}$$

$$Acceleration \begin{cases} \ddot{x_1} = l_1 cos\theta_1 \ddot{\theta_1} - l_1 sin\theta_1 (\dot{\theta_1})^2 \\ \ddot{y_1} = -l_1 sin\theta_1 \ddot{\theta_1} - l_1 cos\theta_1 (\dot{\theta_1})^2 \\ \ddot{x_2} = l_1 cos\theta_1 \ddot{\theta_1} - l_1 sin\theta_1 (\dot{\theta_1})^2 + l_2 cos\theta_2 \ddot{\theta_2} - l_2 sin\theta_2 (\dot{\theta_2})^2 \\ \ddot{y_2} = -l_1 sin\theta_1 \ddot{\theta_1} - l_1 cos\theta_1 (\dot{\theta_1})^2 - l_2 sin\theta_2 \ddot{\theta_2} - l_2 cos\theta_2 (\dot{\theta_2})^2 \end{cases} \tag{23}$$

$$Forces \begin{cases} F_{x1} + F_{x2} = m_1 \ddot{x_1} \\ F_{y1} + F_{y2} = m_1 \ddot{y_1} + m_1 g \\ F_{x2} = m_2 \ddot{x_2} \\ F_{x2} = m_2 \ddot{y_2} + m_2 g \end{cases} \tag{24}$$

$$Moments \begin{cases} \tau_1 = (m_1 + m_2) l_1^2 \ddot{\theta_1} + m_2 l_1 l_2 (cos(\theta_1 - \theta_2) \ddot{\theta_1} - sin(\theta_1 - \theta_2) \dot{\theta_2}^2) - m_1 g l_1 sin\theta_1 \\ \tau_2 = m_2 l_2^2 \ddot{\theta_2} + m_2 l_1 l_2 (cos(\theta_1 - \theta_2) \ddot{\theta_2}) + sin(\theta_1 - \theta_2) \dot{\theta_2}^2 - m_2 g sin\theta_2) \end{cases} \tag{25}$$

3.5 Newton Euler computation

In this section we need to program the code to calculate the dynamics of the human motion from the Newton-Euler equations. We will then test, in the next section, the validity of the human model and the hypotheses made, by comparing the computation of the ground reaction force to the measured data. All the calculations are made in the absolute frame.

3.5.1 Parameters and hypothesis for Newton Euler computation

We are using the Newton-Euler equations to compute the dynamics of the Human Body.
For this we first need to make a few assumptions. First, we consider the body segments as rigid bodies having their mass density homogeneously distributed. Secondly, we neglect all the effects of possible loss of energies such as friction or heat transfer, thus the body is a conservative system. Moreover we consider that for each movement needing the two feet on the ground for support, the ground reaction forces applied on the two feet are equal.
In the code of the Newton Euler equations, the inputs needed are the mass, the center of mass and the inertia matrix from each segment computed in the Hanavan Model with the measured BSP.
The output that will be studied is the ground reaction forces that we will compare with the one measured in the experiment to validate our hypothesis.

3.5.2 General NE equations for one body at a given instant

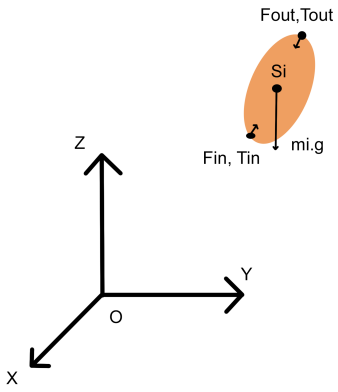

Figure 21: Torques applied on one body

Newton-Euler equations are:

$$\mathbf{F}_{in} + \mathbf{F}_{out} + m_i\mathbf{g} = m_i\dot{\mathbf{V}}_i \tag{26}$$

and

$$\boldsymbol{\tau}_{\text{in}} + \boldsymbol{\tau}_{\text{out}} + \mathbf{r_{in}} \wedge (\mathbf{F_{in}}) + \mathbf{r_{out}} \wedge (\mathbf{F_{out}}) = I_i\dot{\boldsymbol{\omega}}_i + \boldsymbol{\omega}_{\text{i}} \wedge (I_i\boldsymbol{\omega}_{\text{i}}) \tag{27}$$

with

$$\mathbf{V}_i = \frac{d\mathbf{OS_i}}{dt}$$

where:

- **F˙out** is the sum of the forces applied by the next bodies to the body i and **F˙in** is the sum of the forces applied by the previous bodies to the body i
- $\boldsymbol{\tau}$ is the sum of the moments applied on the body i
- $\mathbf{g}$ is the gravity vector
- $\mathbf{r}_{out}$ is the distance between the point of application of the external forces coming from the next body and the center of mass S_i
- $\mathbf{r}_{in}$ is the same for the external forces coming from the previous body.

The elements $\mathbf{F}_{in}$, $\mathbf{F}_{out}$, $\boldsymbol{\tau}_{\text{in}}$ and $\boldsymbol{\tau}_{\text{out}}$ are described in Fig. (21).
The Newton-Euler equations give:

$$\mathbf{F}_{out} = -\mathbf{F}_{in} - m_i\mathbf{g} + m_i\dot{\mathbf{v}}_i \tag{28}$$

and

$$\boldsymbol{\tau}_{out} = -\boldsymbol{\tau}_{in} - \mathbf{r}_{in} \wedge (\mathbf{F}_{in}) - \mathbf{r}_{out} \wedge (\mathbf{F}_{out}) + I_i\dot{\boldsymbol{\omega}}_i + \boldsymbol{\omega}_i \wedge (I_i\boldsymbol{\omega}_i) \tag{29}$$

3.5.3 NE equations for specific segments

Arm Legs and arms are considered as 3 serial bodies. The model of the arm is shown in Fig. (22)

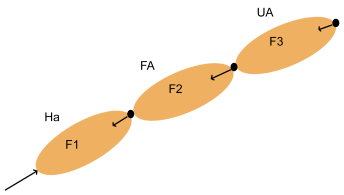

Figure 22: Arm schematic

$$H_q \begin{cases} \mathbf{F_1} = m_{H_q}\mathbf{v\dot{H}_q} - m_{H_q}\mathbf{g} \\ \boldsymbol{\tau}_1 = \mathbf{I_{H_q}}\boldsymbol{\omega}_{\text{H˙q}} + \boldsymbol{\omega}_{\text{H˙q}} \wedge (\mathbf{I_{H_q}}\boldsymbol{\omega}_{\text{H˙q}}) - \mathbf{r_1} \wedge \mathbf{F_1} \end{cases} \tag{30}$$

$$FA \begin{cases} \mathbf{F_2} = m_{FA}\mathbf{v\dot{FA}} + \mathbf{F_1} - m_{FA}\mathbf{g} \\ \boldsymbol{\tau}_2 = \mathbf{I_{FA}}\boldsymbol{\omega}_{\text{FA}} + \boldsymbol{\omega}_{\text{FA}} \wedge (\mathbf{I_{FA}}\boldsymbol{\omega}_{\text{FA}}) + \mathbf{r_1} \wedge \mathbf{F_1} - \mathbf{r_1} \wedge \mathbf{F_1} + \boldsymbol{\tau}_1 \end{cases} \tag{31}$$

$$UA \begin{cases} \mathbf{F_3} = m_{UA}\mathbf{v\dot{UA}} + \mathbf{F_2} - m_{UA}\mathbf{g} \\ \boldsymbol{\tau}_3 = \mathbf{I_{UA}}\boldsymbol{\omega}_{\text{UA}} + \boldsymbol{\omega}_{\text{UA}} \wedge (\mathbf{I_{UA}}\boldsymbol{\omega}_{\text{UA}}) + \mathbf{r_2} \wedge \mathbf{F_2} - \mathbf{r_3} \wedge \mathbf{F_3} + \boldsymbol{\tau}_2 \end{cases} \tag{32}$$

Legs The model of the leg is shown in Fig. (23)

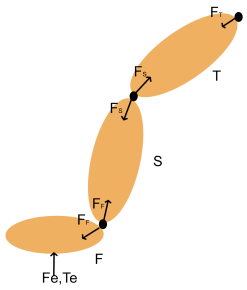

Figure 23: Leg schematic

$$T \begin{cases} \mathbf{F_S} = m_T \dot{\mathbf{v}}_\mathbf{T} - m_T \mathbf{g} + \mathbf{F_T} \\ \boldsymbol{\tau}_\mathrm{S} = \mathbf{I_T}\boldsymbol{\omega}_\mathrm{T} + \boldsymbol{\omega}_\mathrm{T} \wedge (\mathbf{I_T}\boldsymbol{\omega}_\mathrm{T}) + \boldsymbol{\emptyset}_\mathrm{T} - \mathbf{r_S} \wedge \mathbf{F_S} + \mathbf{r_T} \wedge \mathbf{F_T} \end{cases} \tag{33}$$

$$S \begin{cases} \mathbf{F_F} = m_S \dot{\mathbf{v}}_\mathbf{S} - m_S \mathbf{g} + \mathbf{F_S} \\ \boldsymbol{\tau}_\mathrm{F} = \mathbf{I_S}\boldsymbol{\omega}_\mathrm{S} + \boldsymbol{\omega}_\mathrm{S} \wedge (\mathbf{I_S}\boldsymbol{\omega}_\mathrm{S}) + \boldsymbol{\emptyset}_\mathrm{S} - \mathbf{r_S} \wedge \mathbf{F_S} - \mathbf{r_F} \wedge \mathbf{F_F} \end{cases} \tag{34}$$

$$F \begin{cases} \mathbf{F_e} = m_F \dot{\mathbf{v}}_\mathbf{F} - m_F \mathbf{g} + \mathbf{F_F} \\ \boldsymbol{\tau}_\mathrm{e} = \mathbf{I_F}\boldsymbol{\omega}_\mathrm{F} + \boldsymbol{\omega}_\mathrm{F} \wedge (\mathbf{I_F}\boldsymbol{\omega}_\mathrm{F}) + \boldsymbol{\emptyset}_\mathrm{F} + \mathbf{r_F} \wedge \mathbf{F_F} - \mathbf{r_e} \wedge \mathbf{F_e} \end{cases} \tag{35}$$

Head The model of the head is shown in Fig. (24)

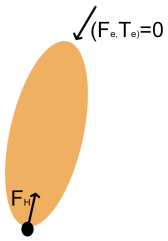

Figure 24: Head schematic

The head is a free independent body.

$$H \begin{cases} \mathbf{F_H} = m_H \dot{\mathbf{v}}_\mathbf{H} - m_H \mathbf{g} \\ \boldsymbol{\tau}_\mathrm{H} = \mathbf{I_H}\boldsymbol{\omega}_\mathrm{H} + \boldsymbol{\omega}_\mathrm{H} \wedge (\mathbf{I_H}\boldsymbol{\omega}_\mathrm{H}) - \mathbf{r_H} \wedge \mathbf{F_H} \end{cases} \tag{36}$$

Upper Trunk The model of the upper trunk is shown in Fig. (25)

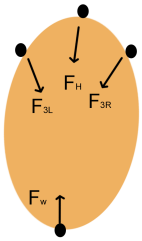

Figure 25: Upper trunk schematic

For the upper part we consider several inputs,but one output body.

$$UT \begin{cases} \boldsymbol{F_\omega} = m_{UT}\mathbf{v\dot{U}T} + \mathbf{F_{3L}} + \mathbf{F_{3R}} + \mathbf{F_H} - m_{UT}\mathbf{g} \\ \boldsymbol{\tau}_\omega = \mathbf{I_{UT}}\boldsymbol{\omega}_{\mathrm{UT}} + \boldsymbol{\omega}_{\mathrm{UT}} \wedge (\mathbf{I_{UT}}\boldsymbol{\omega}_{\mathrm{UT}}) + \mathbf{r_{3L}} \wedge \mathbf{F_{3L}} + \mathbf{r_{3R}} \wedge \mathbf{F_{3R}} + \mathbf{r_H} \wedge \mathbf{F_H} \\ \quad +\boldsymbol{\tau}_{3\mathrm{L}} + \boldsymbol{\tau}_{3\mathrm{R}} + \boldsymbol{\tau}_{\mathrm{H}} - \boldsymbol{r_\omega} \wedge \boldsymbol{F_\omega} \end{cases} \tag{37}$$

Lower Trunk The model of the lower trunk is shown in Fig. (26)

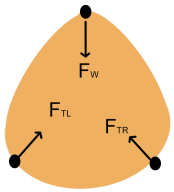

Figure 26: Lower Trunk schematic

For the lower part we consider only one input but several outputs body

$$\mathbf{F}_{T_{L1}} + \mathbf{F}_{T_{R1}} = 0 \tag{38}$$

$$\mathbf{F}_{T_{L2}} = \mathbf{F}_{T_{R2}} \tag{39}$$

$$LT \begin{cases} 2\boldsymbol{F_{T_L}} = m_{LT}\mathbf{v\dot{L}T} - m_{LT}\mathbf{g} + F_w \\ 2\boldsymbol{\tau}_L = \mathbf{I_{LT}}\boldsymbol{\omega}_{\mathrm{LT}} + \boldsymbol{\omega}_{\mathrm{LT}} \wedge (\mathbf{I_{LT}}\boldsymbol{\omega}_{\mathrm{LT}}) + \mathbf{r_w} \wedge \mathbf{F_w} + \boldsymbol{\tau}_{\mathrm{w}} \end{cases} \tag{40}$$

4 Analysis

4.1 Objectives and protocol

So far we have computed the ground reaction forces using two different methods, applying Newton Euler equations from the top of the body to the ground, or assuming the human body is behaving like an inverted or a double inverted pendulum.
We have also explained that the motions performed by the actors were monitored and recorded by two devices. One of these two devices, the force plate Dtrack, was used to compute the ground reaction forces and moments applied. The objective is to apply the motion recorded on a human body to control a humanoid robot or its simulation.
We assumed the density to be constant in all the parts of the body and the forces to be shared equally in both of the legs while in double support. This assumption was made because we couldn't know in which direction the weight is distributed. The aim of this section is to analyse if our assumptions are correct and if our protocol to apply human motion on humanoid control is valid. From the data given of the recorded forces and moments, we can compare them with those we computed. We can thus deduce if the hypothesis we made are correct and decide if our method of recording human motion to apply it for humanoid control is valid or not.

4.2 Joints forces and moments of the ground reaction

We recorded and analysed several motions of various dynamics, some slow motions, some fast, some complex or not. The aim is too analyse all of those motions reaction forces and moments comparing those computed from Newton Euler top to bottom approach and those recorded with the force plate device.

4.2.1 Observation and analyse of a simple motion ground reaction forces and moments

The most simple motion we had available is the waving motion that is shown in figure 13.

Observations The ground reaction forces associated to this motion are compared in figure 27.

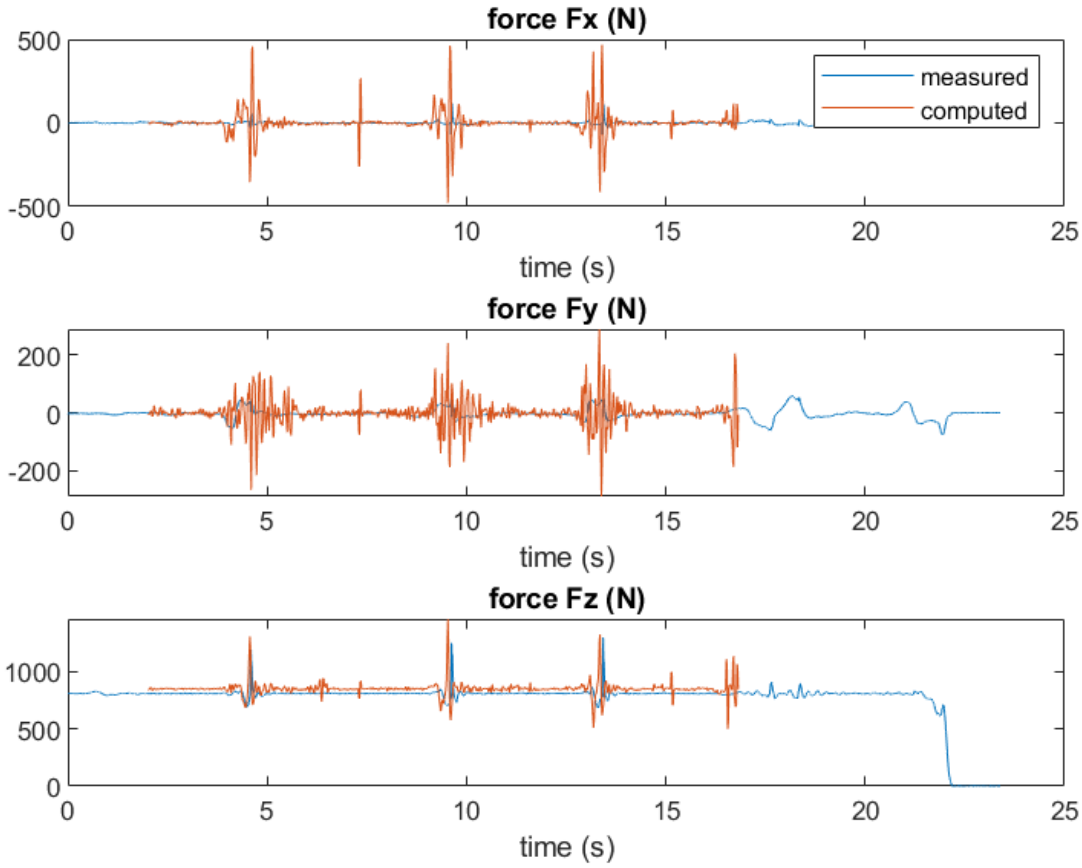

Figure 27: Arm slow motion - Forces

Three elements we have to be compared are:

- the shape of the two curves
- the occurrence of peaks of amplitude
- the amplitude

There is a little shift in time between the two measured and computed curves, which we have partly fixed using an offset value written in the Matlab code. Regarding the force along the z axis, which is the most important ground reaction force we computed, and probably the most accurate one since it shouldn't be too much impacted by our assumptions and should be the easiest to record using the device:

- The shape observed for the measured and computed curves are quite similar: they are both nearly constant with regular peaks of amplitude. However the computed one has a lot of additional small peaks.
- The occurrence of the highest peaks is about the same for both curves. They happen at the same time. However for the lower peaks the computed curves have more of them: especially 3 ones at the right of the graph that are still of high amplitude and not observed on the measured curve.

- The amplitudes of the highest peaks that can be observed in both curves are similar although they are a bit higher for the computed curve.

Regarding the forces along the x and y axis it can be observed:

- The shape is similar in the sense that both curves are constant with peaks happening at the same instant
- The occurrences are a bit different since, if the instant of peaks are similar, the number of peaks is very different as there are a lot more peaks in the computed curve
- The amplitude of the peaks is very different. It is of approximately 500 N along the x axis for the computed signal and of approximately 50 N for the measured one. Along the y axis it is of about 200 N for the highest peak of the computed signal. It is of about 50 N for the measured curve.

The moments of the ground reaction are observed and compared in the figure 28.

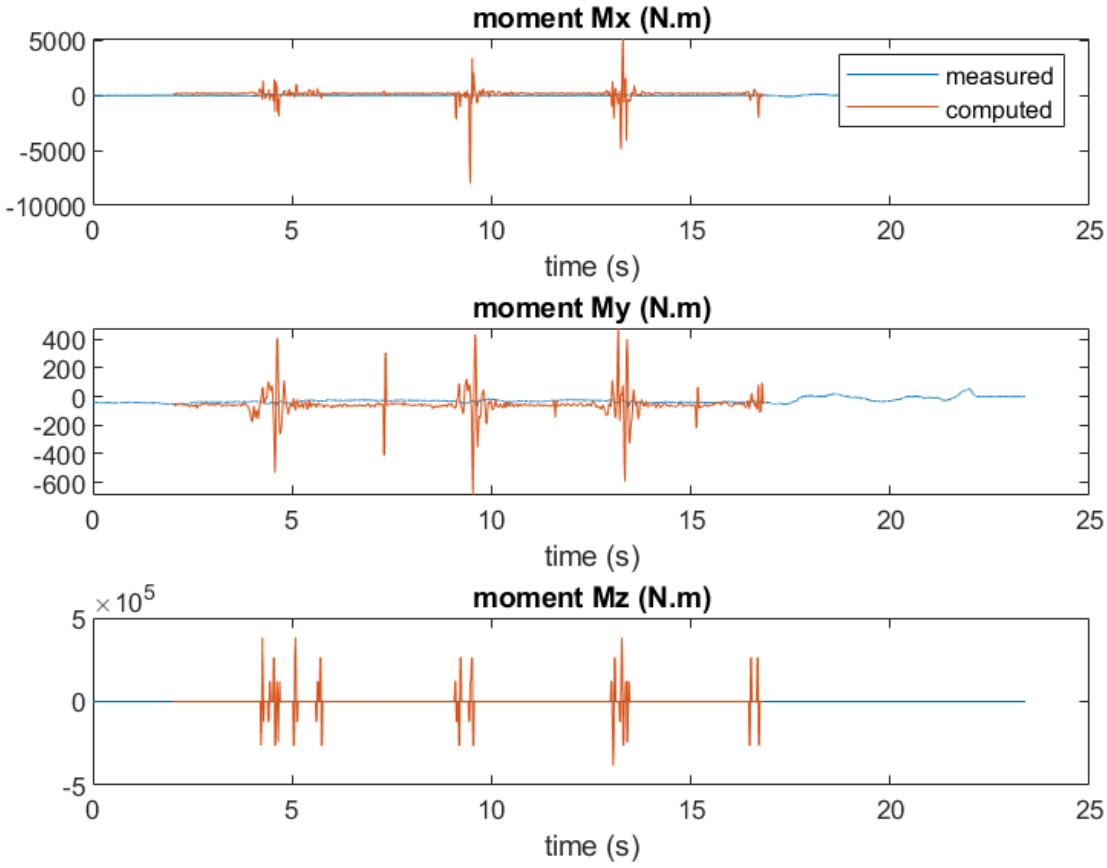

Figure 28: Arm slow motion - Moments

Regarding all the moment comparison it can be observed that:

- the shapes of the computed and measured moments are very different since the measured moment seems to be at zero during the whole motion

- for the same reason the occurrences and amplitude of the peaks observed are also very different

Analysis Globally the motion can be recognised using the ground reaction force along the z axis. Indeed the curves are similar in terms of shape, occurrences and amplitudes. However we do notice differences. The offset of amplitude is probably due to the way the weight was estimated in our computations. Moreover the differences in shape and occurrences are probably due to the fact that the ground reaction forces should be filtered because of accelerations peaks. Regarding the reaction forces along the y axis and the x axis, the motion is more difficult to recognised with the obtained results. Indeed the differences between the two signals are too big. This is not surprising taken into consideration the fact that we made a lot of assumptions, especially regarding the way the mass is distributed throughout the body. Those results show us that those assumptions were maybe too strong and could be better to improve our results. Those differences are even more important as soon as we have motions of high dynamics. This is what is studied in the next part.
Regarding the moments nothing can be deduced clearly from the measured motions. There might be a problem in the recording of the motion or in our use of it. The comparison can't be used to validate our model and hypothesis.

4.2.2 Observation and analyse of a simple motion with high and slow velocity ground reaction forces and moments

To understand the effect of velocity and acceleration on our model results we need to choose a simple motion performed at two different speed. We select the waving motion. This motion was recorded at slow, medium and fast velocity, after making sure they were performed in a nearly identical manner to try to identify the effect of the difference of speed between them.

Observation of the waving arm ground reaction forces and moments at high velocity In Fig (27) and (29) we show the waving arm motion ground reaction forces along the three axes for two different velocities: slow and fast.
We can observe that the forces curves for the slow motion are very similar as previously described. Regarding the fast motion of the arm it can be observed that:

- The shapes of the ground reaction forces along the z axis are fairly similar. The shapes of the ground reaction forces along the x and y axis are very different.
- The occurrence is higher for the computed reaction forces along every axis with a ratio of approximately 20 peaks of amplitude in 18 seconds for the computed ground reaction forces to approximately 3 peaks of amplitude in 18 seconds for the measured ground reaction forces.
- The amplitudes are close for the forces measured and computed along the z axis. They are five to ten times smaller for the measured forces along the x and y axes than for the computed reaction forces along those same axes.

We can also observe that, as previously, the computed moments for the fast motion are very different than the measured ones in shape, occurrences and amplitude.

Analysis From these observations we can deduce that, as before, the most accurate computed force is the one along the z axis. The assumptions we are doing have a lot of impact on the differences between computed and measured motions. Other than for the ground reaction force along the z axis, the hypothesis are not valid. The motion can only be recognised by matching the curves of the ground reaction force along the z axis. The higher the velocity is and the worst is the impact of our assumptions on the accuracy of our results. One possible explanation for the observed differences and the impact made by the modification of velocity is that it can cause discontinuities in acceleration creating unwanted peaks in the computed forces. Indeed for high velocity motions the markers can be missed at some instants. It would be an interesting improvement to filter those peaks. However we have to make sure that the filtering is only removing unwanted peaks and is not deleting important data. This is a difficult process that has to be done carefully and that would require another complete analysis to properly be applied. For such reason we decided not to do this and to keep in mind the effect of acceleration discontinuities.

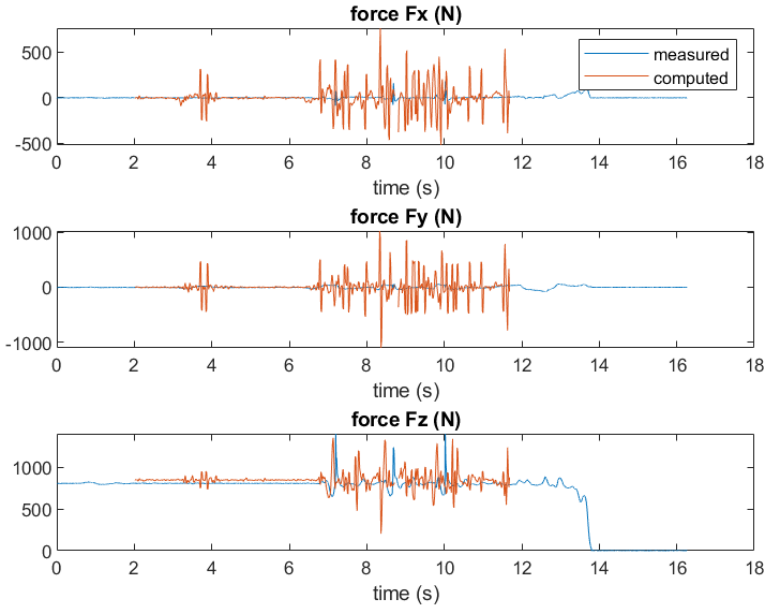

Figure 29: Arm fast motion - Forces

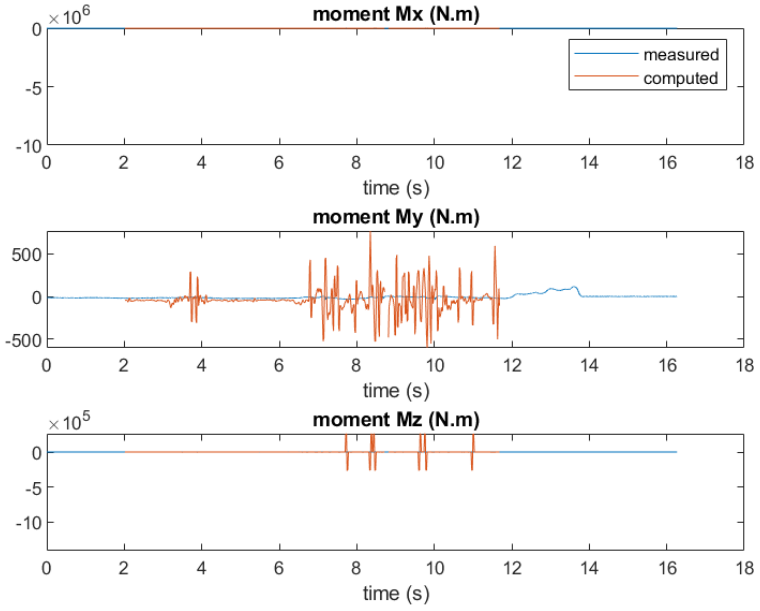

Figure 30: Arm fast motion - Moments

The apparition of peaks due to acceleration discontinuities can also be observed for complex motions. We select the custom motion that can be observed in figure 14. It is interesting to remind that the visualisation of this motion was already made complicated by the absence of part of the data due to markers concealing. In that sense many acceleration discontinuities and differences between the measured and the computed signals are expected.

4.2.3 Observation and analysis of a complex motion, the custom one, ground reaction forces and moments

Observation In Fig (31) and (32) we show the custom motion ground reaction forces and moments.
Regarding the ground reaction forces and moments it can be observed that:

- The shapes of the ground reaction forces and moments along all the axes are very different, even for the force along the z axes. While measured data don't show much variation in moments and forces for the ground reaction, the computed data are affected by many very high peaks in amplitude going up to 1200 N for the force along the z axis.
- The occurrence of these peaks is much higher for the computed reaction forces and moments than for the measured ones along every axes. The ratio can't be computed as the peaks for the measured data are not visible. However approximately 30 peaks of amplitude in 18 seconds can be observed for the computed ground reaction forces. This is more than what is observed for a simple motion.
- The amplitudes are extremely high for the computed data in forces and moments.

Analysis From these observations we can deduce that, as before, data are made wrong by many discontinuities in acceleration. These discontinuities have also been observed in the

similation since some markers stoped being tracked at some instants of the simulation. It reinforce the idea that those peaks due to acceleration discontinuities have to be filtered to be able to correctly analyse our data and to validate or not our model.

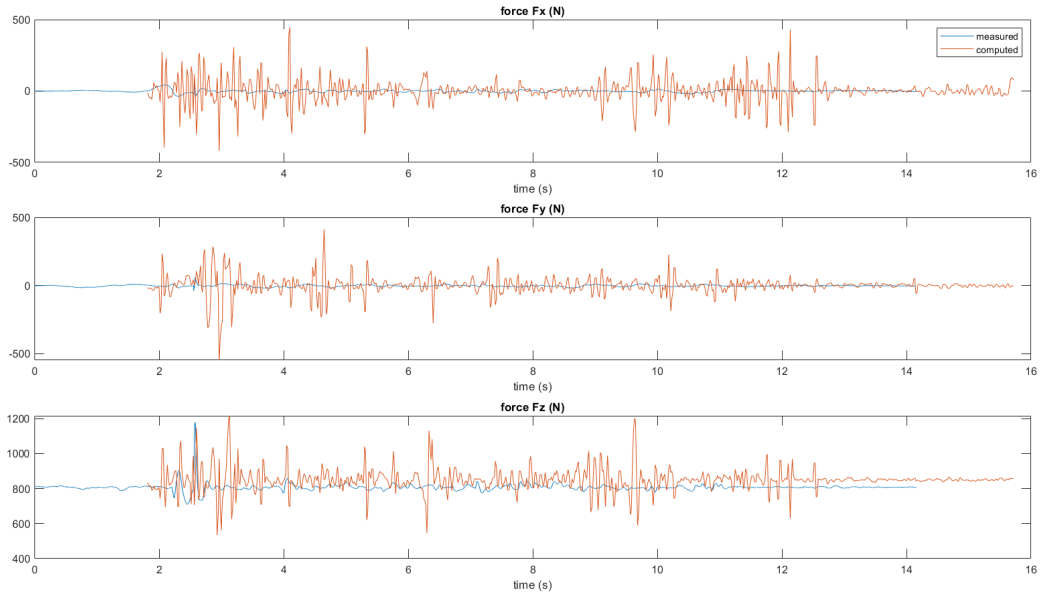

Figure 31: Custom motion - Forces

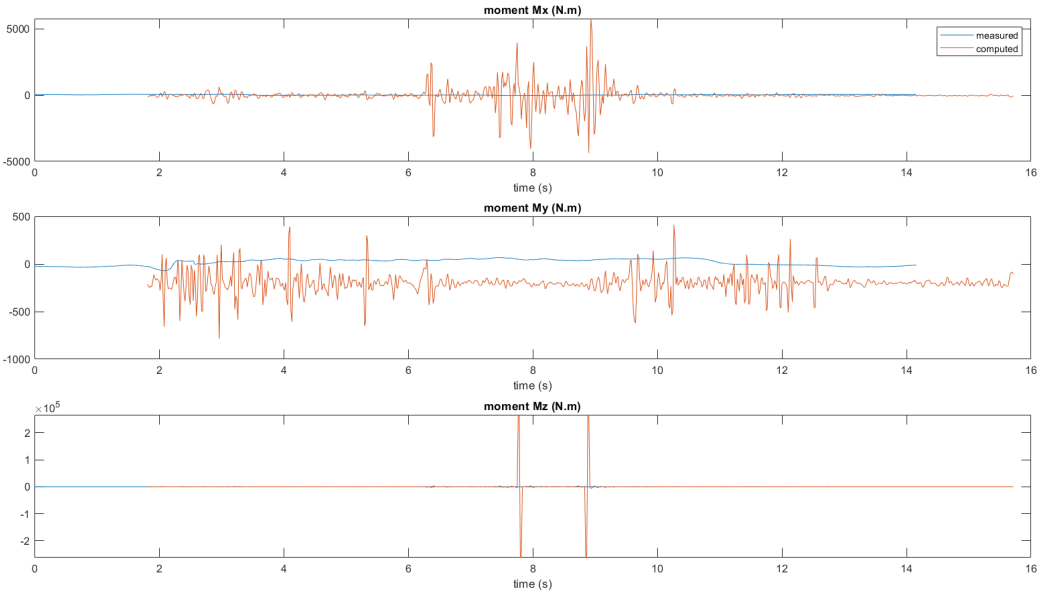

Figure 32: Custom - Moments

5 Synthesis

This report shows how to modelize a human body and how to animate it using motions recorded from on a motion capture system. From our data analysis, comparing the computed and measured data, we were able to deduce that the model we have implemented still suffers from imperfections.
The computations we made can be considered correct only for the ground reaction force along the z axis. The proposed method to compute the efforts can be used to estimate the ground reaction forces for motions in a slow and medium speed motion. The model and assumptions being made can't be validated at the end of our project. However filtering the discontinuities in acceleration, that, we believe, disturb the data, may better drastically the obtained results and may validate our model and hypothesis.

A Repository organisation

The code repository is organised as follows:

- *ForceData* → it contains all the data files provided with the subject
- *Hanavan_model* → it contains the scripts for the construction of the model from the Hanavan parameter
- *NE* → it contains scripts which apply the Newton-Euler algorithm to compute the ground reaction forces and bodies moments
- *animation* → it contains the script permitting to have a visualisation of the motions
- *motion_data* → .drf data motions files
- *motions* → data motions files converted in .mat

How to run the code In order to run the code one need first to select the name of the motion they want to execute in the Matlab file *run.m* as shown in Fig (33) (line 30 in the file)

```
Motion = "slowArm";

animation =  true; % true or false
```

Figure 33: Run.m

To choose the correct motion write the corresponding name of the data file. For example, to simulate the motion of the arm at slow speed, write:

Motion = ”slowArm”

For the other motions, the correct names to insert are listed in the comments of the file *run.m* We are then required to set the correct offset value in the file *plot_ground_reaction.m* in order to visualise the computed and measured graphs correctly (line 22, see Fig (34)). For example

```
k = size(F_Grnd,2) ;
f = 1/60;
t = 2 +  (f:f:(f*k));%add offse here: change the offset here to match with force data
```

Figure 34: Run.m

we may use the following offset values:

- 2 for *fastArm*
- 2 for *slowArm*
- 2 for *fastArm*
- 1.8 for *fastKick*

- 2.1 for *fastKickArm*
- 1.4 for *mediumKick*
- 1.5 for *mediumKickArm*
- 1.5 for *slowKick*
- 1.8 for *fastKick*
- 1 for *JumpFeetUp*

Before running the *main.m* and depending on the type of motion, we also need to choose between *double_support.m*, for example for jumping, sitting, waving hand, or *single_support.m* (line 27). We should use *mix_support.m* for the custom motions Once changed all these values we can run the file *main.m*

N.B. A last minute version of the code was added in hmhc_latestVersion. This version was made to be easier to launch the whole project, since it only requires to run *main.m* file after deciding the motion to study. There might be bugs, so we decided to upload the previous version also hmhc_checkedVersion. To run the previous version, follow the instructions above.